Experimental Line Parameters of the $b^1\Sigma_g^+ \leftarrow X^3\Sigma_g^-$ Band of Oxygen Isotopologues at 760 nm Using Frequency-Stabilized Cavity Ring-Down Spectroscopy†

David J. Robichaud, Laurence Y. Yeung, David A. Long, and Mitchio Okumura*

Division of Chemistry and Chemical Engineering, California Institute of Technology, Pasadena, California 91125

Daniel K. Havey and Joseph T. Hodges*

Process Measurements Division, National Institute of Standards and Technology, 100 Bureau Drive, Gaithersburg, Maryland 20899

Charles E. Miller* and Linda R. Brown*

Jet Propulsion Laboratory, California Institute of Technology, 4800 Oak Grove Drive, Pasadena, California 91109

Received: February 6, 2009; Revised Manuscript Received: May 22, 2009

Positions, intensities, self-broadened widths, and collisional narrowing coefficients of the oxygen isotopologues $^{16}O^{18}O$, $^{16}O^{17}O$, $^{17}O^{18}O$, and $^{18}O^{18}O$ have been measured for the $b^1\Sigma g + \leftarrow X^3\Sigma g -$ (0,0) band using frequency-stabilized cavity ring-down spectroscopy. Line positions of 156 P-branch transitions were referenced against the hyperfine components of the ^{39}K D_1 ($4s\ ^2S_{1/2} \rightarrow 4p\ ^2P_{1/2}$) and D_2 ($4s\ ^2S_{1/2} \rightarrow 4p\ ^2P_{3/2}$) transitions, yielding precisions of ~0.00005 cm^{-1} and absolute accuracies of 0.00030 cm^{-1} or better. New excited $b^1\Sigma g +$ state molecular constants are reported for all four isotopologues. The measured line intensities of the $^{16}O^{18}O$ isotopologue are within 2% of the values currently assumed in molecular databases. However, the line intensities of the $^{16}O^{17}O$ isotopologue show a systematic, *J*-dependent offset between our results and the databases. Self-broadening half-widths for the various isotopologues are internally consistent to within 2%. This is the first comprehensive study of the line intensities and shapes for the $^{17}O^{18}O$ or $^{18}O_2$ isotopologues of the $b^1\Sigma g + \leftarrow X^3\Sigma g -$ (0,0) band of O_2. The $^{16}O_2$, $^{16}O^{18}O$, and $^{16}O^{17}O$ line parameters for the oxygen A-band have been extensively revised in the HITRAN 2008 database using results from the present study.

1. Introduction

The oxygen A-band, $b^1\Sigma g + \leftarrow X^3\Sigma g -$ (0,0), is the most prominent near-infrared feature in the Earth's atmosphere. It has been used extensively since the 1960s to determine cloud top heights, cloud optical properties, and aerosol optical thickness.[1] Such studies have been extended to the A-band spectra from the GOME[2] and SCIAMACHY[3,4] satellite instruments. Minor isotopologue bands, particularly $^{16}O^{18}O$ and $^{16}O^{17}O$, significantly overlap with the $^{16}O_2$ A-band and can bias retrieval of atmospheric data if the line parameters are not accurately known.[5] The 2004 edition of HITRAN[6] reports line positions based on the 1948 study by Babcock and Herzberg[7] for $^{16}O^{18}O$ and assumes intensities and lineshape parameters to be equivalent to the corresponding $^{16}O_2$ band. The $^{16}O^{17}O$ positions, intensities, and broadening parameters are based on the balloon spectra of Camy-Peyret.[8]

Since Babcock and Herzberg's original work[7] on $^{16}O_2$, $^{16}O^{17}O$, and $^{16}O^{18}O$, there have been surprisingly few studies of the $b^1\Sigma g + \leftarrow X^3\Sigma g -$ (0,0) isotopologue spectra.[7−12] Recent work was largely motivated by testing for violations of the symmetrization postulate of quantum mechanics.[10,11] Naus et al.[11] used cavity ring-down spectroscopy to study the line positions of all six isotopologues with 0.03 cm^{-1} accuracy. Nearly simultaneously, Gagliardi and co-workers[10] were the first to investigate the $b^1\Sigma g + \leftarrow X^3\Sigma g -$ (0,0) spectrum of $^{18}O_2$. They used frequency modulation (FM) diode-laser spectroscopy to measure line positions for transitions up to $J'' = 13$ (where J'' denotes the total angular momentum of the ground state) to measure line positions with uncertainties of 0.0001 cm^{-1}. Schermaul[12] studied the intensities, line positions, and pressure-broadening widths of the $^{16}O^{18}O$ isotopologue using a "collisionally narrowed Voigt profile." Camy-Peyret et al.[8] used atmospheric balloon spectra to determine positions and intensities for the $^{16}O^{17}O$ isotopologue. Finally, van Leeuwen et al.[9] studied the intensities and positions of 17 high-*J* $^{16}O^{18}O$ transitions using noise-immune cavity-enhanced optical heterodyne molecular spectroscopy (NICE-OHMS). To our knowledge, there have been no comprehensive studies of the line intensities or shapes for the $^{17}O^{18}O$ or $^{18}O_2$ isotopologues of the $b^1\Sigma g + \leftarrow X^3\Sigma g -$ (0,0) band of O_2. Table 1 summarizes the results of previous studies.

The present study extends our previous work on the $^{16}O_2$ A-band[13−15] to the $^{16}O^{17}O$, $^{16}O^{18}O$, $^{17}O^{18}O$, and $^{18}O_2$ isotopologues using frequency-stabilized cavity ring-down spectroscopy (FS-CRDS). The $^{17}O_2$ transitions, although present in our spectra, were too weak to provide accurate line position or line shape determinations. We present transition frequencies, intensities, and line shape parameters for each isotopologue and compare our results to previous measurements where available. These experiments form the basis for the revised values of the $^{16}O_2$, $^{16}O^{18}O$, and $^{16}O^{17}O$ line parameters of the oxygen A-band presently found in HITRAN 2008.

† Part of the "Robert W. Field Festschrift".

10.1021/jp901127h CCC: $40.75
Published on Web 07/08/2009

TABLE 1: Summary of Isotopologue Studies of the O_2 $b^1\Sigma g + \leftarrow X^3\Sigma g -$ (0, 0) Band

study	year	technique[a]	isotopologues	no. of lines	position uncertainty, cm^{-1}
current study	2009	FS-CRDS	$^{16}O^{17}O$, $^{16}O^{18}O$, $^{17}O^{18}O$, $^{18}O_2$	156	<0.0003
van Leeuwen et al.[9]	2004	NICE-OHMS	$^{16}O^{18}O$	17	0.02
Camy-Peyret[8]	2000	balloon	$^{16}O^{17}O$, $^{16}O^{18}O$		
Schermaul[12]	1999	FTS	$^{16}O^{18}O$	71	0.001
Naus et al.[11]	1997	CRDS	$^{16}O^{17}O$, $^{16}O^{18}O$, $^{17}O^{18}O$, $^{18}O_2$, $^{17}O_2$	340	0.03
Gagliardi et al.[10]	1997	FM-diode	$^{18}O_2$	15	0.01
Babcock and Herzberg[7]	1948	atmos inter.	$^{16}O^{17}O$, $^{16}O^{18}O$	119	0.01

[a] FS-CRDS, frequency-stabilized cavity ring-down spectroscopy; balloon, atmospheric FTS balloon instrument; FTS, Fourier transform spectroscopy; FM-diode, frequency modulation-diode laser spectroscopy; CRDS: cavity ring-down spectroscopy; atmos inter., atmospheric spectra using interferometry.

TABLE 2: Composition of the ^{18}O-Enriched Gas Sample

	natural abundance[a]	calculated, supplier[b]	mass spectrometer[c]	spectral intensities[d]
$^{16}O_2$	0.995262	0.2098	0.2784 (51)	0.2705 (18)
$^{16}O^{18}O$	0.00399141	0.4827	0.3672 (18)	0.3769 (49)
$^{16}O^{17}O$	0.000742	0.0137	0.0099 (4)	
$^{18}O_2$	4.00178×10^{-6}	0.2777	0.3271 (32)	
$^{17}O^{18}O$	1.49×10^{-6}	0.0158	0.0174 (4)	
$^{17}O_2$	1.38×10^{-7}	0.0002	not determined	

[a] Based on HITRAN 2004[6] recommended values. [b] The supplier provided enrichment data in atom percentages: $^{16}O = 45.8\%$, $^{17}O = 1.5\%$, $^{18}O = 52.7\%$. Abundance values in the "supplier" column were calculated assuming a stochastically distributed sample. [c] Isotopologue determination by mass spectrometer. The $^{16}O^{18}O$ value is actually the sum of the $^{16}O^{18}O + {}^{17}O_2$ (i.e., mass = 34). Values in parentheses are 1σ uncertainty of the last digit. [d] Determined from line intensity measurements relative to $^{16}O_2$.

2. Experimental Apparatus

The FS-CRDS spectrometer located at the National Institute of Standards and Technology (NIST), Gaithersburg, MD, has been described in detail.[13−20] The ring-down cavity mirrors used in this study had nominal transmission losses of 200 ppm (finesse ~15000) centered at 13050 cm^{-1} and the cavity length was nominally 74 cm. The system noise-equivalent absorption coefficient was approximately 6×10^{-10} cm^{-1} $Hz^{-1/2}$. Ring-down decays, having typical decay times of 4−12 μs, were measured using an 8 MHz Si-PIN photodetector and fit using the algorithm of Halmer et al.[21] Ring-down decay times less than 4 μs suffered from nonlinear effects in the absorption signal due to the bandwidth of the photodetector. This limited the high end of the pressure range used for individual transitions. Pressures greater than 133 Pa (1 Torr) were used to minimize the influence of pressure gauge uncertainties on our intensity measurements.

Spectra of $^{16}O^{17}O$, $^{16}O^{18}O$, $^{17}O^{18}O$, and $^{18}O_2$ were recorded using an ^{18}O-enriched sample (see Table 2 for gas sample composition information). The temperature was measured using a NIST-calibrated 2.4 kΩ thermistor in thermal contact with the outer wall of the absorption cell. Temperatures ranged from 295 to 298 K. No effort was made to stabilize or control the temperature of the cell; the temperature typically varied by less than 1.5 K during the course of a single day. Gas pressure was measured with two NIST-calibrated capacitance diaphragm gauges having full scale responses of 13.3 kPa (100 Torr) and 133 kPa (1000 Torr), respectively, and readout accuracies of better than 0.01%. An overview of the experimental conditions is given in Table 3.

Spectral scans from 12975 to 13110 cm^{-1} were recorded with a nominal step size of 202 MHz (0.00674 cm^{-1}), the cavity free-spectral range (FSR). A portion of the spectrum is shown in Figure 1. Absolute line positions were referenced against the hyperfine components of the ^{39}K D_1 ($4s\ ^2S_{1/2} \rightarrow 4p\ ^2P_{1/2}$) and D_2 ($4s\ ^2S_{1/2} \rightarrow 4p\ ^2P_{3/2}$) transitions as described previously for the $^{16}O_2$ A-band transitions.[15] Due to the importance of $^{16}O^{18}O$ in atmospheric retrievals, 10 GHz wide microwindows centered on selected transitions were rescanned with a 50 MHz step size to improve the precision of line intensity and line shape measurements. Note the Doppler full width half-maximum

TABLE 3: Experimental Conditions[a]

Isotopologue	Data Set	P(kPa)	Scan Range	Step Size (MHz)	Mirror Loss (ppm)	Scan Time
$^{16}O^{18}O$, $^{16}O^{17}O$, $^{18}O_2$, and $^{17}O^{18}O$	A	0.1339	(12975−13115) cm^{-1}	202	200	1 day
	B	1.329	(12975−13078) cm^{-1}			
	C	3.281	(12975−13076) cm^{-1}			
	D	7.979	(12975−13086) cm^{-1}			
$^{16}O^{18}O$	E	100.0	(8−12) GHz[b]	50	20	10 min
	F	60.02	(8−12) GHz[b]			
	G	39.82	(8−12) GHz[b]			
	H	19.36	(8−12) GHz[b]			
	I	13.37	(8−12) GHz[b]			
	J	9.215	(8−12) GHz[b]			
	K	5.273	(8−12) GHz[b]			
	L	2.080	(8−12) GHz[b]			
	M	1.190	(8−12) GHz[b]			
	N	0.680	(8−12) GHz[b]			
	O	0.324	(8−12) GHz[b]			
	P	2.750	(8−12) GHz[b]	(50, 100)	20	10 min
	Q	22.20	(8−12) GHz[b]			

[a] All scans were performed using an ^{18}O-enriched sample (see Table 2 for composition). [b] These data sets were centered on individual transitions. All measurements were made at temperatures near 296 K.

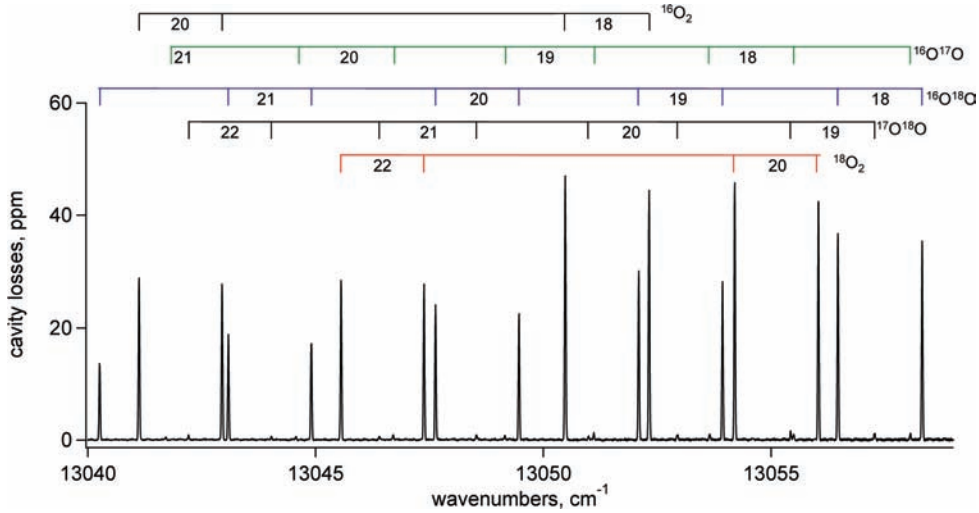

Figure 1. Recorded absorption spectrum of the PP and PQ branches of the O_2 A-band with empty cavity losses and Rayleigh scattering subtracted. Sample pressure is 133.9 Pa (1.004 Torr) ^{18}O-enriched gas at 296.0 K (data set A). Isotopologue assignments shown at top, where upper state J is listed between PP (left) and PQ (right) lines.

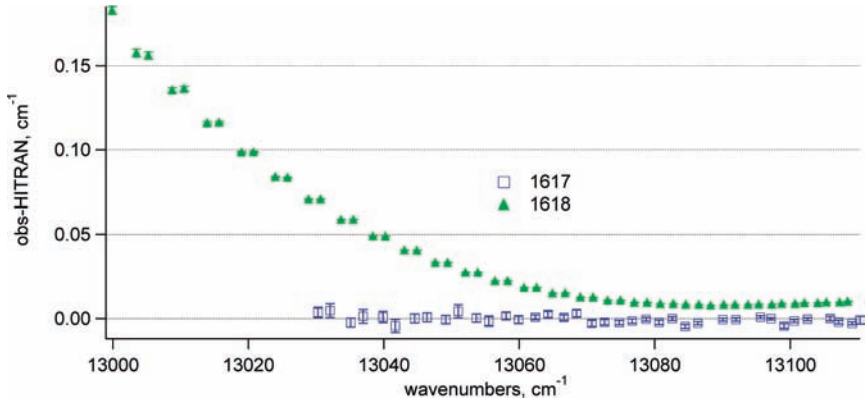

Figure 2. Differences between observed $^{16}O^{17}O$ and $^{16}O^{18}O$ transition line positions and HITRAN 2004 values.[6] The $^{16}O^{18}O$ and $^{16}O^{17}O$ values originated from Babcock and Herzberg[7] and Camy-Peyret et al.,[8] respectively.

(fwhm) of $^{16}O^{18}O$ in this spectral region is ~830 MHz (0.0275 cm^{-1}) at 296 K. To conserve the ^{18}O-enriched gas sample during pressure studies, the cell was charged once to 101.3 kPa (760 Torr) and then successively evacuated to achieve lower pressures. All transitions were fit using a Galatry[22] line shape, a soft-collision approximation that generalizes the Voigt profile for Dicke narrowing effects. Line intensities, pressure-induced broadening, and collisional narrowing coefficients were fitted to minimize the differences between the observed and calculated spectra. All of the scans recorded for pressures >5.33 kPa (40 Torr) exhibited the asymmetric residuals characteristic of speed-dependent line shape effects. Preliminary analyses indicated that the errors from neglecting speed dependence were less than 0.1%. A detailed study of speed-dependent effects in the oxygen A-band will be the subject of a future report. Line mixing was not considered in the present study.

To confirm experimental reproducibility, several of the $^{16}O^{18}O$ and the majority of the $^{16}O^{17}O$ measurements were repeated using the same ^{18}O-enriched sample and lower loss cavity mirrors (~20 ppm losses, centered at 13072 cm^{-1}). The noise-equivalent absorption coefficient was improved to 1×10^{-10} cm^{-1} $Hz^{-1/2}$ with these low loss mirrors and decay times increased to 20−80 μs. Microwindow scans (10 GHz wide) centered on these transitions were performed. The $^{16}O^{18}O$ spectra were recorded at 2.75 kPa (20.8 Torr) with a step size of 50 MHz. $^{16}O^{17}O$ spectra were recorded at 22.2 kPa (167 Torr) with a 50 MHz step size for $J' = 25-29$ and a step size of 100 MHz for $J' = 17-24$. All other experimental details were identical to those described above.

3. Results and Discussion

Line positions, intensities, pressure broadened widths, and narrowing coefficients for $^{18}O_2$, $^{16}O^{18}O$, $^{16}O^{17}O$, and $^{17}O^{18}O$ are presented in Tables 4−7, respectively. A detailed analysis of $^{17}O_2$ was not performed, because the $^{17}O_2$ transitions were either too weak for accurate measurement or obscured by the transitions of the more abundant isotopologues in our spectra.

A. Line Positions. The $b^1\Sigma g + \leftarrow X^3\Sigma g -$ band is electric dipole forbidden by both spin and orbital angular momentum selection rules, but it is allowed by magnetic dipole selection rules.[7] The rotational levels of the O_2 states are described by the angular momentum quantum numbers N and J, where N is the rotational angular momentum, S is the spin angular momentum, and J is the total angular momentum, $J = N + S$. The $X^3\Sigma g -$ state is split into three levels, $J'' = N'' - 1$, N'', and $N'' + 1$ while the $b^1\Sigma g +$ state has only levels $J' = N'$. For the symmetric isotopologues with nuclear spin of zero, $^{16}O_2$ and $^{18}O_2$, only the odd levels of N in the $X^3\Sigma g -$ electronic state and the even levels in the $b^1\Sigma g +$ state are allowed due to spin statistics. All rotational states are allowed for the asymmetric isotopologues $^{16}O^{17}O$, $^{16}O^{18}O$, and $^{17}O^{18}O$. The $b^1\Sigma g + \leftarrow X^3\Sigma g -$ band comprises four types of transitions represented by ΔN N'' ΔJ J'', limited to PP, PQ, RQ, and RR. This study focused

TABLE 4: Measured Line Parameters of the $^{16}O^{18}O$ Isotopologue[a]

assignment $\Delta N\ N''\ \Delta J\ J''$	position[b] (cm^{-1})	unc (10^{-5} cm^{-1})	obs-calc (10^{-5} cm^{-1})	J'	intensity[c]	% unc	γ,[d] HWHM	α[d]
P3 P3	13114.57458	*		2	11.081	0.50		
P4 Q3	13113.62672	*		3	9.904	0.90		
P4 P4	13111.59661	*		3	13.157	0.50		
P5 Q4	13110.53627	*		4	11.771	0.50		
P5 P5	13108.53136	(7)	0	4	14.755	0.49		
P6 Q5	13107.36492	(3)	1	5	13.171	0.50		
P6 P6	13105.37891	(3)	−1	5	15.902	0.49		
P7 Q6	13104.10978	(3)	0	6	14.072	0.49		
P7 P7	13102.13927	(4)	−2	6	16.586	0.49		
P8 Q7	13100.76953	(4)	1	7	14.559	0.49		
P8 P8	13098.81251	(4)	0	7	16.796	0.49		
P9 Q8	13097.34351	(3)	−1	8	14.638	0.49		
P9 P9	13095.39862	(3)	−2	8	16.596	0.49		
P10 Q9	13093.83126	(3)	4	9	14.302	0.49		
P10 P10	13091.89770	(4)	5	9	15.991	0.49		
P11 Q10	13090.23265	(5)	0	10	13.613	0.49		
P11 P11	13088.30924	(4)	−2	10	15.366	0.50		
P12 Q11	13086.54727	(4)	2	11	12.715	0.49		
P12 P12	13084.63442	(4)	2	11	13.988	0.49		
P13 Q12	13082.77522	(4)	−1	12	11.636	0.49		
P13 P13	13080.87217	(4)	−2	12	12.649	0.49		
P14 Q13	13078.91623	(5)	−5	13	10.444	0.49		
P14 P14	13077.02268	(5)	−5	13	11.303	0.73		
P15 Q14	13074.97025	(5)	−2	14	9.253	0.57	0.0138 (2)	
P15 P15	13073.08601	(5)	2	14	9.962	0.52	0.0141 (2)	
P16 Q15	13070.93727	(6)	−2	15	7.968	0.51	0.0138 (3)	
P16 P16	13069.06217	(6)	−6	15	8.585	0.50	0.0138 (1)	
P17 Q16	13066.81709	(6)	5	16	6.820	0.48	0.0134 (1)	
P17 P17	13064.95086	(6)	−1	16	7.266	0.48	0.0141 (4)	
P18 Q17	13062.60969	(8)	8	17	5.702	0.49	0.0134 (1)	0.002 (6)
P18 P18	13060.75228	(7)	8	17	6.062	0.47	0.0131 (1)	0.002 (5)
P19 Q18	13058.31486	(8)	6	18	4.689	0.49	0.0136 (1)	0.001 (4)
P19 P19	13056.46624	(7)	5	18	4.976	0.48	0.0133 (1)	0.002 (4)
P20 Q19	13053.93247	(10)	−1	19	3.801	0.47	0.0129 (1)	0.003 (4)
P20 P20	13052.09249	(9)	4	19	4.016	0.47	0.0130 (1)	0.003 (4)
P21 Q20	13049.46240	(10)	−2	20	3.031	0.46	0.0125 (1)	0.002 (4)
P21 P21	13047.63103	(9)	14	20	3.193	0.46	0.0128 (1)	0.003 (3)
P22 Q21	13044.90461	(10)	−13	21	2.380	0.46	0.0125 (1)	0.003 (3)
P22 P22	13043.08186	(10)	7	21	2.474	0.68	0.01252 (3)	0.003 (1)
*P*23 Q22	13040.25880	(11)	−6	22	1.826	0.60	0.01220 (1)	0.003 (4)
*P*23 *P*23	13038.44454	(9)	−17	22	1.926	0.98	0.01240 (3)	0.004 (1)
P24 Q23	13035.52511	(12)	6	23	1.392	0.50	0.01213 (3)	0.004 (2)
P24 P24	13033.71893	(12)	4	23	1.453	0.06	0.01225 (3)	0.004 (3)
P25 Q24	13030.70321	(16)	−22	24	1.041	0.57	0.01200 (1)	0.004 (2)
P25 P25	13028.90547	(18)	17	24	1.086	0.55	0.01198 (3)	0.004 (1)
P26 Q25	13025.79249	(24)	−17	25	0.773	0.51	0.01180 (3)	0.0046 (1)
P26 P26	13024.00348	(27)	−24	25	0.803	0.62	0.01210 (5)	0.0049 (1)
P27 Q26	13020.79349	(42)	25	26	0.561	0.71	0.01180 (3)	0.0046 (1)
P27 P27	13019.01229	(47)	−4	26	0.583	0.68	0.01183 (3)	0.0049 (1)
P28 Q27	13015.70605	(68)	101	27	0.405	0.49	0.01126 (3)	0.0043 (1)
P28 P28	13013.93287	(80)	17	27	0.421	0.47	0.01144 (4)	0.0049 (1)
P29 Q28	13010.52992	(135)	−86	28	0.289	1.03	0.01078 (1)	0.0043 (1)
P29 P29	13008.76441	(154)	62	28	0.296	0.67	0.01102 (1)	0.0047 (3)
P30 Q29	13005.26189	(216)	177	29	0.199	1.00	0.01061 (1)	0.0042 (1)
P30 P30	13003.50690	(230)	149	29	0.204	1.96	0.01045 (4)	0.0039 (1)
P31 Q30	12999.90889	(233)	372	30	0.139	1.43	0.01050 (20)	
P31 P31	12998.15880	*		30	0.1419	0.56	0.01059 (1)	0.0048 (1)
P32 Q31	12994.46173	*		31	0.0934	0.53	0.01039 (1)	0.0049 (1)
P32 P32	12992.72156	*		31	0.0959	1.14	0.01028 (2)	0.0046 (1)
P33 Q32	12988.92634	*		32	0.0624	1.12	0.00998 (3)	0.0045 (1)
P33 P33	12987.19430	*		32	0.0674	0.44	0.01027 (3)	0.0050 (1)
P34 Q33	12983.30068	*		33	0.0439	0.91	0.00980 (3)	0.0043 (2)
P34 P34	12981.57674	*		33	0.0416	1.92	0.00986 (5)	0.0046 (2)
P35 Q34	12977.58444	*		34	0.0265	0.75	0.00974 (7)	0.0043 (5)
P35 P35	12975.86859	*		34	0.0274	1.09	0.00944 (5)	0.0033 (4)

[a] The values in parentheses (1σ uncertainty of the last digits) are type A uncertainties and quantify the precision and reproducibility of the measurement. They are based on the quadrature sum of the fitted parameter uncertainties obtained by the Galatry line shape fits and the standard deviation of repeated measurements. These uncertainties do not account for systematic effects associated with the line shape model but do incorporate uncertainty in the isotope abundance as shown in Table 3 for the intensities. Combined relative standard uncertainties in S_i associated with the measurement of p, T, composition, and spectral frequency axes are estimated to be <0.2%. Intensities and shape parameters for $J \geq 24$ are based on data sets E−O. [b] Positions in cm^{-1}, transitions denoted with an asterisk (*) are calculated values and not used in the fit to determine the molecular constants. [c] Intensities are in units of 10^{-27} cm^{-1}/(molecules cm^{-2}) at $T = 296$ K, adjusted for natural abundance (0.00399141). [d] Pressure broadening (γ) and collisional narrowing (α) coefficients are in units of MHz/Pa (note 3.3798 cm^{-1}/atm = 1 MHz/Pa).

TABLE 5: Measured Line Parameters of the $^{18}O_2$ Isotopologue[a]

assignment $\Delta N\ N''\ \Delta J\ J''$	position[b]	unc (10^{-5} cm^{-1})	obs-calc (10^{-5} cm^{-1})	J'	intensity[c]	% unc	γ,[d] HWHM	α[d]
P5 Q4	13113.50532	*		4	23.373	0.42		
P5 P5	13111.50822	*		4	26.587	0.06		
P7 Q6	13107.45947	(6)	1	6	25.818	0.06		
P7 P7	13105.49276	(3)	6	6	30.166	0.04		
P9 Q8	13101.09288	(3)	−15	8	27.082	0.05		
P9 P9	13099.14936	(3)	3	8	30.624	0.08		
P11 Q10	13094.40203	(3)	0	10	25.654	0.06		
P11 P11	13092.47827	(3)	0	10	28.299	0.05		
P13 Q12	13087.38493	(3)	2	12	22.277	0.06		
P13 P13	13085.47950	(3)	3	12	24.218	0.06		
P15 Q14	13080.04082	(3)	−1	14	18.026	0.07		
P15 P15	13078.15275	(3)	0	14	19.299	0.08		
P17 Q16	13072.36906	(4)	−1	16	13.638	0.27	0.0137 (2)	
P17 P17	13070.49778	(3)	1	16	14.475	0.23	0.0126 (2)	
P19 Q18	13064.36895	(5)	1	18	9.686	0.11	0.0140 (1)	
P19 P19	13062.51401	(4)	1	18	10.217	0.07	0.0125 (2)	
P21 Q20	13056.03963	(6)	−7	20	6.470	0.04	0.0126	
P21 P21	13054.20068	(6)	−2	20	6.787	0.04	0.0135 (1)	
P23 Q22	13047.38018	(7)	−6	22	4.068	0.02	0.0121 (1)	0.003 (3)
P23 P23	13045.55718	(6)	1	22	4.253	0.02	0.0120 (1)	0.0018 (3)
P25 Q24	13038.38972	(7)	4	24	2.414	0.04	0.0119 (2)	0.003 (3)
P25 P25	13036.58230	(9)	7	24	2.513	0.03	0.0118 (1)	0.0033 (3)
P27 Q26	13029.06678	(10)	−5	26	1.355	0.07	0.0114 (1)	0.0041 (3)
P27 P27	13027.27477	(10)	11	26	1.402	0.07	0.0113 (1)	0.0036 (3)
P29 Q28	13019.40991	(23)	−26	28	0.722	0.13	0.0113 (2)	0.005 (1)
P29 P29	13017.63324	(25)	−1	28	0.746	0.13	0.0111 (2)	0.005 (1)
P31 Q30	13009.41764	(68)	−21	30	0.363	0.27	0.0090 (7)	0.002 (1)
P31 P31	13007.65711	(75)	33	30	0.376	0.26	0.0101 (7)	0.004 (1)
P33 Q32	12999.09087	(215)	134	32	0.176	0.56	0.0105 (15)	0.007 (4)
P33 P33	12997.34441	(232)	202	32	0.180	1.11	0.0099 (18)	0.007 (4)
P35 Q34	12988.42071	*		34	0.078	1.28	0.0099 (21)	0.003 (4)
P35 P35	12986.69015	*		34	0.080	1.25	0.0078 (18)	0.001 (4)
P37 Q36	12977.41169	*		36	0.033	3.03	0.0063 (25)	
P37 P37	12975.69630	*		36	0.033	3.03	0.0056 (25)	

[a] Intensities for $J \leq 14$ are based on data set A only. Intensities for $J \geq 23$ are based on data sets B−D. [b] Positions in cm^{-1}, transitions denoted with an asterisk (*) are calculated values and not used in the fit to determine the molecular constants. [c] Intensities are in units of 10^{-30} cm^{-1}/(molecules cm^{-2}) at $T = 296$ K, adjusted for natural abundance (4.00178×10^{-6}). [d] Pressure broadening (γ) and collisional narrowing (α) coefficients are in units of MHz/Pa. The values in parentheses (1σ uncertainty of the last digits) are described in Table 4.

on the P-branch where PP- and PQ-type transitions form doublets with a splitting of approximately 2 cm^{-1}.

Absolute transition frequencies were calibrated using the hyperfine components of ^{39}K D lines as described previously.[15] Since accurate pressure shift parameters are not known for any of the rare oxygen isotopologues, all transition frequencies were corrected using the corresponding pressure shift parameters for $^{16}O_2$;[13] the shift coefficients were interpolated for odd values of J'. This approximation should not affect the reported positions since pressure shift parameters are not expected to change much with isotopic substitution, and the $\sim 10^{-5}$ cm^{-1} pressure shifts at 133 Pa were smaller than the measured position uncertainties.

Line positions for each isotopologue were incorporated into a least-squares fitting routine to derive molecular constants. The Hamiltonian of Rouillé et al.[23] was used for the $X^3\Sigma g^-$ ($\nu = 0$) ground state, while the $b^1\Sigma g^+$ ($\nu = 0$) excited state was modeled with

$$E = T + BJ(J+1) - DJ^2(J+1)^2 + HJ^3(J+1)^3 \quad (1)$$

Accurate ground state constants were previously determined for $^{18}O_2$, $^{16}O^{18}O$, $^{16}O^{17}O$, and $^{17}O^{18}O$.[23−26] These are listed in Table 8 and were held fixed while fitting for the upper state constants. Molecular constants for the $b^1\Sigma g^+$ states are presented in Table 9 along with values from previous studies. Constants for $^{16}O_2$ previously reported by Robichaud et al.[15] are shown for comparison. To maintain consistency with the database, the ground state energy levels for the $^{16}O_2$ and $^{18}O_2$ isotopologues are set relative to the $N'' = 1$, $J'' = 0$ level, whereas the energy levels of the $^{16}O^{17}O$, $^{16}O^{18}O$, and $^{17}O^{18}O$ isotopologues are given relative to the $N'' = 0$, $J'' = 1$ level. Where necessary, we recalculated the $b^1\Sigma g^+ \leftarrow X^3\Sigma g^-$ band origins reported in Table 9 to account for this ground state energy convention. We note that HITRAN 2004 did not scale the $^{16}O^{17}O$ $X^3\Sigma g^-$ energy levels in this manner.

The frequencies for the strongest $^{16}O^{18}O$ and $^{18}O_2$ transitions were measured with uncertainties of 1 MHz (3×10^{-5} cm^{-1}); frequencies for weaker $^{16}O^{18}O$ and $^{18}O_2$ transitions or transitions, associated with the less abundant $^{16}O^{17}O$ and $^{17}O^{18}O$ isotopologues, were measured with correspondingly larger uncertainties (Tables 4−7). These accuracies are comparable to those observed in our study of the $^{16}O_2$ spectrum.[15] The observed−calculated (o-c) residuals, determined using the constants in Tables 8 and 9, are generally much smaller than the stated 1σ uncertainties and never exceed 2σ.

Figure 2 compares the atmospherically important $^{16}O^{17}O$ and $^{16}O^{18}O$ transition frequencies from the present work with HITRAN 2004.[6] The $^{16}O^{17}O$ transition frequencies, derived from the atmospheric balloon spectra of Camy-Peyret et al.,[8] agree within ± 0.002 cm^{-1} and exhibit no significant systematic differences. In contrast, the $^{16}O^{18}O$ transition frequencies,

TABLE 6: Measured Line Parameters of the $^{16}O^{17}O$ Isotopologue[a]

assignment $\Delta N\ N''\ \Delta J\ J''$	position[b]	unc (10^{-4} cm^{-1})	o-c (10^{-4} cm^{-1})	J'	intensity[c] 200 ppm	% unc	intensity[c] 20 ppm	% unc	intensity[c] merged	% unc
P4 Q3	13112.3406	*		3	2.18	5.96			2.18	5.96
P4 P4	13110.3054	(23)	−2	3	2.73	5.49			2.73	5.49
P5 Q4	13109.1627	(9)	−11	4	2.32	5.60			2.32	5.60
P5 P5	13107.1554	(11)	−2	4	3.01	4.98			3.01	4.98
P6 Q5	13105.90454	(13)	3	5	2.69	6.31			2.69	6.31
P6 P6	13103.9160	*		5						
P7 Q6	13102.5587	(9)	7	6	2.68	5.22			2.68	5.22
P7 P7	13100.5861	(8)	−5	6	3.43	4.66			3.43	4.66
P8 Q7	13099.1254	(15)	−3	7	2.56	7.03			2.56	7.03
P8 P8	13097.1684	(7)	6	7	3.37	4.74			3.37	4.74
P9 Q8	13095.6049	(8)	3	8	2.93	5.11			2.93	5.11
P9 P9	13093.6593	*		8						
P10 Q9	13091.9948	(10)	0	9	2.74	5.10			2.74	5.10
P10 P10	13090.0608	(9)	−6	9	3.17	4.73			3.17	4.73
P11 Q10	13088.2964	*		10						
P11 P11	13086.3739	(9)	−1	10	3.12	4.80			3.12	4.80
P12 Q11	13084.5091	(12)	2	11	2.48	4.03			2.48	4.03
P12 P12	13082.5971	(11)	2	11	2.71	4.05			2.71	4.05
P13 Q12	13080.6310	(13)	−12	12	2.31	3.89			2.31	3.89
P13 P13	13078.7304	(12)	0	12	2.46	3.65			2.46	3.65
P14 Q13	13076.6656	(13)	−6	13	2.035	4.02			2.035	4.02
P14 P14	13074.7748	(13)	6	13	2.159	4.02			2.159	4.02
P15 Q14	13072.6115	(17)	6	14	1.775	4.00			1.775	4.00
P15 P15	13070.7268	(18)	−18	14	1.883	4.03			1.883	4.03
P16 Q15	13068.4684	(21)	23	15	1.543	4.01			1.543	4.01
P16 P16	13066.5936	(17)	3	15	1.611	4.03			1.611	4.03
P17 Q16	13064.2322	(18)	4	16	1.286	4.04			1.286	4.04
P17 P17	13062.3685	(14)	4	16	1.365	4.02			1.365	4.02
P18 Q17	13059.9083	(22)	5	17	1.071	4.01			1.071	4.01
P18 P18	13058.0554	(22)	22	17	1.131	3.97			1.131	3.97
P19 Q18	13055.4933	(30)	−6	18	0.874	4.00			0.874	4.00
P19 P19	13053.6478	(24)	−6	18	0.921	4.01			0.921	4.01
P20 Q19	13050.9949	(39)	47	19	0.718	4.03			0.718	4.03
P20 P20	13049.1530	(25)	−6	19	0.736	3.94	0.730	0.22	0.731	0.20
P21 Q20	13046.3970	(27)	5	20	0.544	4.04	0.552	0.28	0.549	0.25
P21 P21	13044.5681	(27)	−6	20	0.573	4.01	0.576	0.49	0.571	0.35
P22 Q21	13041.7071	(38)	−56	21	0.438	3.88	0.427	0.39	0.430	0.32
P22 P22	13039.8929	(33)	−8	21	0.442	3.84	0.431	0.24	0.432	0.22
P23 Q22	13036.9375	(41)	−10	22	0.324	4.01	0.337	0.86	0.325	0.55
P23 P23	13035.1230	(27)	−52	22	0.343	3.79	0.333	0.15	0.333	0.16
P24 Q23	13032.0748	(41)	9	23	0.249	4.01	0.247	0.32	0.247	0.31
P24 P24	13030.2716	(31)	−6	23	0.269	4.08	0.252	0.15	0.252	0.17
P25 Q24	13027.1186	*		24	0.187	3.74	0.187	0.18	0.187	0.23
P25 P25	13025.3256	*		24	0.202	3.96	0.190	0.18	0.189	0.22
P26 Q25	13022.0726	*		25	0.132	4.54	0.135	0.19	0.135	0.30
P26 P26	13020.2881	*		25	0.130	5.38	0.138	0.12	0.137	0.29
P27 Q26	13016.9356	*		26	0.095	6.31	0.099	0.32	0.100	0.51
P27 P27	13015.1596	*		26	0.107	7.47	0.098	0.35	0.098	0.57
P28 Q27	13011.7075	*		27	0.081	9.87	0.069	2.00	0.068	2.27
P28 P28	13009.9400	*		27	0.073	12.3	0.070	0.29	0.069	0.81
P29 Q28	13006.3880	*		28	0.061	11.4	0.049	0.18	0.049	1.25
P29 P29	13004.6289	*		28	0.039	15.3	0.048	0.28	0.048	1.24
P30 Q29	13000.9768	*		29	0.034	26.4	0.034	1.14	0.035	3.08
P30 P30	12999.2262	*		29	0.030	30	0.034	1.15	0.034	3.5

[a] The values in parentheses (1σ uncertainty of the last digits) are described in Table 4. Intensities for $J \leq 13$ are based on data set A only. Intensities for $J \geq 23$ are based on data sets B−D. [b] Positions in cm^{-1}, transitions denoted with an asterisk (*) are calculated values and not used in the fit to determine the molecular constants. [c] Intensities are in units of 10^{-27} cm^{-1}/(molecules cm^{-2}) at $T = 296$ K, adjusted for natural abundance (0.000742). Pressure broadening (γ) and collisional narrowing (α) coefficients are in units of MHz/Pa.

derived from the 1948 Babcock and Herzberg data[7] (the $^{16}O^{18}O$ positions were not updated in HITRAN 2004 using ref 8 despite what is written in ref 6), deviate by +0.01 cm^{-1} at low J and differences increase to 0.3 cm^{-1} at $J = 34$. Similar discrepancies were also noted by van Leeuwen et al.[9]

B. Comparisons of Line Positions. The only other study to determine molecular constants for the set of minor isotopologues is that of Naus et al.[11] Their work used cavity ring-down spectroscopy and reported line position accuracies of 0.03 cm^{-1}. Despite the larger uncertainties, their molecular constants are in generally good agreement (within 2σ uncertainty) with the current work. Babcock and Herzberg[7] reported a centrifugal distortion constant, D, for the $^{16}O^{18}O$ isotopologue significantly larger than that determined in the current work, in Schermaul,[12] and also in van Leeuwen et al.[9] The deviation in the distortion constant is consistent with the observed discrepancies between our observed positions and those listed in HITRAN 2004, where the discrepancy

TABLE 7: Measured Line Parameters of the $^{17}O^{18}O$ Isotopologue[a]

assignment $\Delta N\ N''\ \Delta J\ J''$	position[b]	unc (10^{-4} cm^{-1})	obs-calc (10^{-4} cm^{-1})	J'	intensity[c]	% unc
P4 Q3	13115.0958	*		3	34.9	3.93
P4 P4	13113.0714	*		3	48.3	3.45
P5 Q4	13112.1029	*		4	42.2	3.72
P5 P5	13110.1022	(12)	3	4	53.9	3.27
P6 Q5	13109.0309	(5)	−4	5	44.6	3.52
P6 P6	13107.0472	(8)	−8	5	57.2	3.08
P7 Q6	13105.8783	(7)	−1	6	49.6	3.96
P7 P7	13103.9090	(7)	−7	6	84.7	6.72
P8 Q7	13102.6434	(5)	5	7	52.5	3.17
P8 P8	13100.6874	(4)	5	7	63.3	2.94
P9 Q8	13099.3239	(5)	−4	8	50.9	3.08
P9 P9	13097.3807	(5)	8	8	61.0	2.89
P10 Q9	13095.9223	(6)	2	9	48.5	3.23
P10 P10	13093.9872	(6)	−13	9	60.4	2.92
P11 Q10	13092.4361	(7)	−1	10	48.4	3.24
P11 P11	13090.5135	(5)	8	10	55.8	2.98
P12 Q11	13088.8668	(7)	5	11	43.9	3.35
P12 P12	13086.9524	(6)	−2	11	52.1	3.01
P13 Q12	13085.2127	(7)	3	12	40.9	3.35
P13 P13	13083.3076	(6)	−5	12	47.2	2.28
P14 Q13	13081.4740	(9)	−5	13	39.9	2.21
P14 P14	13079.5795	(7)	3	13	42.4	2.31
P15 Q14	13077.6506	(9)	−16	14	35.7	2.19
P15 P15	13075.7652	(8)	−6	14	37.1	2.38
P16 Q15	13073.7472	(11)	17	15	30.6	2.24
P16 P16	13071.8680	(9)	0	15	32.3	2.43
P17 Q16	13069.7541	(11)	−4	16	26.0	2.26
P17 P17	13067.8855	(11)	−0	16	27.4	2.15
P18 Q17	13065.6798	(15)	9	17	21.9	2.24
P18 P18	13063.8192	(13)	8	17	23.1	2.12
P19 Q18	13061.5161	(17)	−26	18	18.2	2.16
P19 P19	13059.6668	(13)	1	18	18.9	2.07
P20 Q19	13057.2727	(18)	−10	19	15.0	2.61
P20 P20	13055.4292	(14)	−9	19	15.4	2.54
P21 Q20	13052.9445	(19)	5	20	12.2	2.41
P21 P21	13051.1091	(17)	6	20	12.5	2.36
P22 Q21	13048.5352	(22)	60	21	9.5	2.06
P22 P22	13046.7031	(19)	12	21	9.9	1.98
P23 Q22	13044.0297	(26)	4	22	7.4	2.66
P23 P23	13042.2085	(22)	−17	22	7.8	2.53
P24 Q23	13039.4454	(48)	14	23	5.68	2.24
P24 P24	13037.6297	(25)	−34	23	5.84	2.35
P25 Q24	13034.7735	*		24	4.40	2.45
P25 P25	13032.9706	*		24	4.41	2.22
P26 Q25	13030.0173	*		25	3.40	2.31
P26 P26	13028.2224	*		25	3.26	2.40
P27 Q26	13025.1753	*		26	2.47	2.77
P27 P27	13023.3884	*		26	2.47	2.77
P28 Q27	13020.2474	*		27	1.85	4.23
P28 P28	13018.4685	*		27	1.87	3.66
P29 Q28	13015.2333	*		28	1.13	6.08
P29 P29	13013.4623	*		28	1.37	6.42
P30 Q29	13010.1329	*		29	0.77	12.8
P30 P30	13008.3698	*		29	1.06	8.33
P31 Q30	13004.9459	*		30	2.51	3.90
P31 P31	13003.1907	*		30	0.60	11.4

[a] The values in parentheses (1σ uncertainty of the last digits) are described in Table 4. Intensities for $J \leq 11$ are based on data set A only. Intensities for $J \geq 23$ are based on data sets B−D. [b] Positions in cm^{-1}, transitions denoted with an asterisk (*) are calculated values and not used in the fit to determine the molecular constants. [c] Intensities are in units of 10^{-31} cm^{-1}/(molecules cm^{-2}) at $T = 296$ K, adjusted for natural abundance (1.49×10^{-6}).

increases quadratically with J. Finally, our results are in excellent agreement with those of Camy-Peyret[8] for the $^{16}O^{17}O$ isotopologue.

C. Isotopologue Composition. Great care was taken to determine accurate isotopologue abundances in the ^{18}O-enriched gas sample (seen in Table 2). The vendor provided ^{16}O, ^{17}O and ^{18}O atom percentage abundances, not the isotopologue fractions that were needed. We therefore performed our own mass spectral analysis using a double-focusing magnetic sector mass spectrometer with electron impact ionization (JEOL JMS-600H). Pure aliquots from each cylinder were introduced into the mass spectrometer with a direct inlet, and mass scans were conducted from $m/z = 32$ to 36. Peak intensities were recorded and used for the

TABLE 8: Molecular Constants for the $X^3\Sigma g^- (v = 0)$ Ground State of O_2[a]

	B_0	$D_0 \times 10^{-6}$	$H_0/10^{-12}$	λ_0	$\lambda_0'/10^{-6}$	$\lambda_0''/10^{-12}$	$\mu_0/10^{-3}$	$\mu'_0/10^{-9}$	$\mu''_0/10^{-14}$	zero level	ref
$^{16}O_2$	1.437676476 (77)	4.84256 (63)	2.8 (16)	1.984751322 (72)	1.94521 (50)	11.03 (41)	−8.425390 (13)	−8.106 (32)	−4.7 (19)	−0.24584	23
$^{16}O^{17}O$	1.395319 (3)	4.623		1.984 7094 (3)	1.917 (6)		−8.17612 (13)	−8.0 (10)		−0.46452	24
$^{16}O^{18}O$	1.35785222 (16)	4.319 (13)		1.98467443 (17)	1.83305 (9)	9.84 (83)	−7.955998 (17)	−7.3177 (13)		−0.47795	25
$^{17}O^{18}O$	1.315490 (3)	4.102		1.9846329 (13)	1.801 (10)		−7.70696 (23)	−9.0 (20)		−0.49403	24
$^{18}O_2$	1.27800847 (23)	3.83		1.98459622 (37)	1.738 (14)		−7.48648 (10)	−11.7 (18)		−0.07516	26

[a] All values in cm^{-1}. The values in parentheses represent the uncertainty in the last significant digit(s). Molecular constants fixed to these values during the fit.

TABLE 9: Molecular Constants for the $b^1\Sigma g^+$ State of Molecular Oxygen

	T (cm^{-1})	B (cm^{-1})	D (10^{-6} cm^{-1})	H (10^{-12} cm^{-1})	ref
$^{16}O_2$	13122.00575 (1)	1.3912496 (1)	5.3699 (3)	−1.8(2)	Robichaud et al.[15]
$^{16}O^{17}O$	13123.8036 (5)	1.350270 (5)	5.109 (8)		this work
	13123.808 (3)	1.350232 (15)	5.07 (2)		Naus et al.[11]
	13123.808 (1)	1.350312 (6)	5.092 (5)		Camy-Peyret[8]
	13123.77 (6)	1.352 0 (1)			Babcock and Herzberg[7]
$^{16}O^{18}O$	13124.79314 (2)	1.3140440 (4)	4.7891 (16)	−4.8 (20)	this work
	13124.797 (7)	1.313 92 (9)	4.4 (2)		Naus et al.[11]
	13124.8027 (9)	1.314031 (14)	4.75 (4)		Schermaul[12]
	13124.8008 (10)	1.314051 (8)	4.808 (8)		van Leeuwen et al.[9]
	13124.795 (1)	1.31412 (1)	5.05 (1)		Babcock and Herzberg[7]
$^{17}O^{18}O$	13125.9282 (3)	1.273070 (4)	4.553 (9)		this work
	13125.924 (8)	1.27319 (8)	4.8 (1)		Naus et al.[11]
$^{18}O_2$	13126.51615 (3)	1.2368158 (4)	4.253 (1)	−2.4 (13)	this work
	13126.4989 (8)	1.236833 (6)	4.255 (8)		Naus et al.[11]
	13126.498 (3)	1.23680 (14)	4.0 (5)		Gagliardi et al.[10]

calculation of isotope abundances. The relative amounts of $^{16}O_2$ ($m/z = 32$), $^{16}O^{17}O$ ($m/z = 33$), $^{16}O^{18}O$ ($m/z = 34$), $^{17}O^{18}O$ ($m/z = 35$), and $^{18}O_2$ ($m/z = 36$) were calculated directly using normalized peak heights, assuming no significant contribution of $^{17}O_2$ to the ion signal at ($m/z = 34$). We estimate the error due to this assumption to be 0.01%. Use of an isotope ratio mass spectrometer may improve the overall reproducibility of the abundance measurement, though improving the overall accuracy requires a reference gas of nominally similar isotope composition. As an additional check, sixteen $^{16}O_2$ and three $^{16}O^{18}O$ lines were studied in both the ^{18}O-enriched sample and pure O_2 near natural abundance. With the measured peak areas, a, and knowledge of the natural abundance of the isotopologue, I_n, the abundance in the ^{18}O-enriched sample, I_e, was determined using the relation $a_n/a_e = I_n/I_e$, where the subscripts n and e refer to the natural abundance and ^{18}O-enriched samples, respectively. On the basis of our previous study,[13] the reproducibility of the line intensities retrieved from spectra recorded over a period of several months had uncertainties of ~0.2%. The spectroscopically determined ratios differ only slightly from the ratios determined mass spectrometrically; the difference is beyond the quadratic sum of the measured 1σ error bars but within the reproducibility of the spectroscopic intensity ratio.

D. Intensities. Line intensities (near natural abundance, see Table 2), in units of cm^{-1}/(molecules cm^{-2}), were corrected to $T = 296$ K using

$$S_i(296\text{ K}) = S_i(T)\frac{q(T)}{q(296\text{ K})}\frac{e^{-E/k(296\text{K})}}{e^{-E/kT}} \quad (2)$$

where $q(T)$ is the total partition function at temperature T, k is Boltzmann's constant, E is the lower state energy level determined from the constants in Table 8, and S_i is the line intensity. Line intensities were corrected to near natural abundance assuming the isotopologue distribution from our mass spectral analysis (Table 2). The values of q(296 K) are 454.8, 2656, 2817, 241.7 for $^{16}O^{18}O$, $^{16}O^{17}O$, $^{17}O^{18}O$, and $^{18}O_2$, respectively.

TABLE 10: Band Strengths of the Oxygen A-Band (in cm^{-1}/cm^{-2} molecule at 296 K)

	no. of lines	instrument type	band strength	
$^{16}O_2$	90		2.28×10^{-22}	HITRAN 2004[6]
	29	FS-CRDS	$2.26(1) \times 10^{-22}$	Robichaud et al.[13]
$^{16}O^{18}O$	140		8.96×10^{-25}	HITRAN 2004[6]
	65	FS-CRDS	$9.1(1) \times 10^{-25}$	this work
	271	FTS	$7.97(3) \times 10^{-25}$	Schermaul[12]
	17		$8(1) \times 10^{-25}$	van Leeuwen et al.[9a]
$^{16}O^{17}O$	140	HITRAN	1.73×10^{-25}	HITRAN 2004[6]
	54	FS-CRDS	$1.9(1) \times 10^{-25}$	this work

[a] Band strength not actually reported, listed band strength is based on average intensity ratio with current work.

To date there are only three measurements of line intensities for the isotopologues of the $b^1\Sigma g^+ \leftarrow X^3\Sigma g^-$ (0,0) band.[8,9,12] Band strengths determined from the current study are compared to those reported by others in Table 10.

For the $^{16}O^{18}O$ isotopologue, Schermaul[12] measured all four branches to $J = 20$ using FTIR, whereas van Leeuwen et al.[9] measured $^{16}O^{18}O$ line intensities from $25 < J < 35$ in the PP and PQ branches using NICE-OHMS. Both studies were performed using O_2 with an isotopic composition near natural abundance and have fairly large uncertainties (on average, 12% and 30% for Schermaul and van Leeuwen et al., respectively). The intensities of the $^{16}O^{18}O$ isotopologue in HITRAN 2004[6] were calculated as described in Gamache et al.[27] and were based on the $^{16}O_2$ band strength of Ritter and Wilkerson,[28] 2.28×10^{-22} cm^{-1}/(molecules cm^{-2}). Line intensities of the current study, Schermaul, and van Leeuwen et al. divided by HITRAN 2004 values are shown in Figure

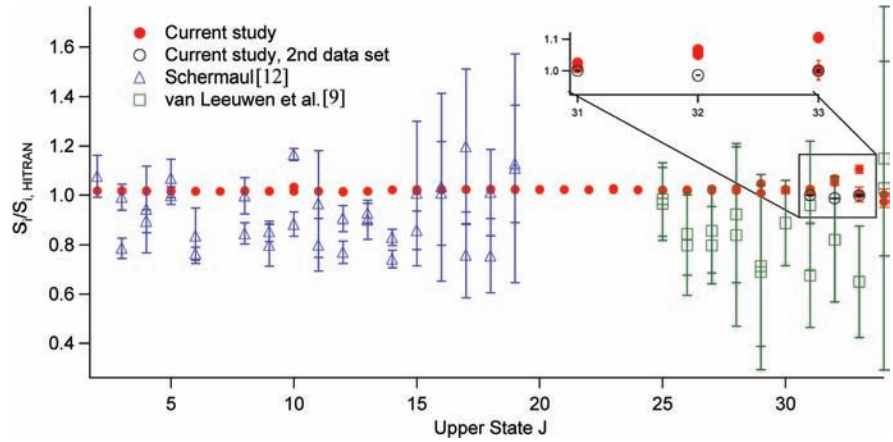

Figure 3. $^{16}O^{18}O$ line intensities divided by HITRAN 2004 values[6] vs J'. Error bars on the current study represent the fit precision (as described in Table 4) and do not incorporate the uncertainty due to the fractionation in the gas sample (<1%).

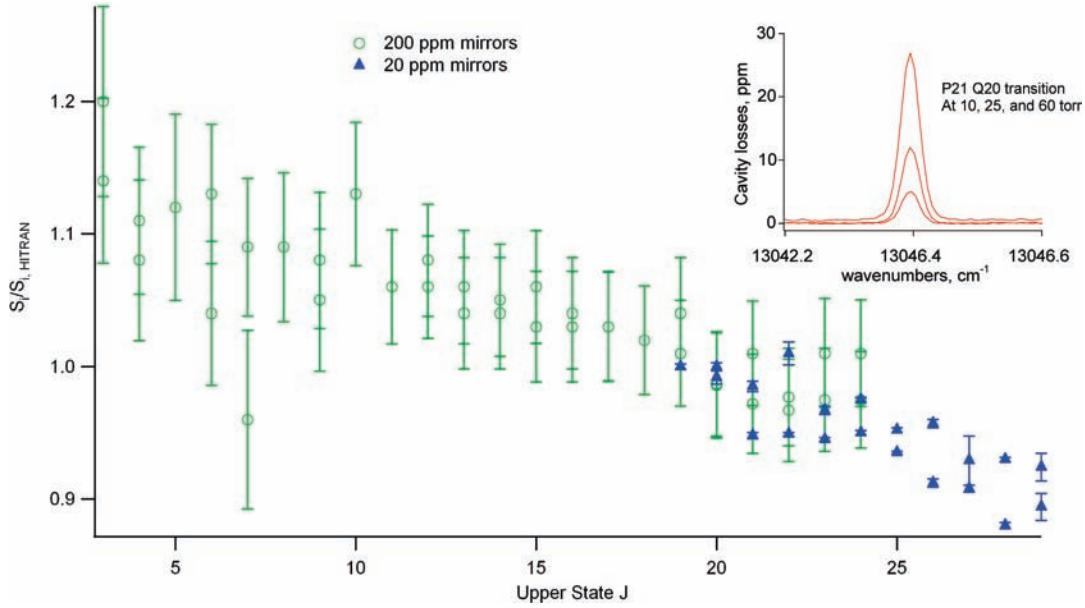

Figure 4. $^{16}O^{17}O$ line intensities divided by HITRAN 2004 values[6] vs J'. Error bars represent the fit precision. Inset shows the P21 Q20 transition at the pressures used for intensity measurements (P = 10, 25, and 60 Torr).

3. While the intensities of Schermaul and van Leeuwen et al. are (7 ± 13)% and (14 ± 13)% lower than those from HITRAN 2004, respectively, the values from the current study are 2.1 (±1.5)% larger.

The intensities of many $^{16}O^{17}O$ transitions were determined by Camy-Peyret et al.[8] from atmospheric balloon spectra. Their results form the basis for the $^{16}O^{17}O$ intensities in HITRAN 2004. Our intensities are compared to those of HITRAN 2004 in Figure 4. The ratios of our $^{16}O^{17}O$ intensities to HITRAN 2004 have a dependence on J; +10% at low J and −10% at J = 28. This is in contrast to the nearly constant offset of the $^{16}O^{18}O$ intensities. To our knowledge, we are the first to report intensities for the $^{17}O^{18}O$ and $^{18}O_2$ isotopologues. To confirm our results, the line intensities of many of the high-J transition were remeasured using 20 ppm mirrors for improved signal-to-noise. As shown in Figure 4, there is no discernible difference between our two data sets.

E. Line Shape Parameters. Self-broadened half-widths (HWHM) are shown in Figure 5. The coefficients for the $^{16}O^{17}O$ and $^{17}O^{18}O$ isotopologues have considerably more uncertainty due to their lower abundances in the gas sample. As is evident, to within a 2% uncertainty there is no difference between pressure broadening coefficients of the various isotopologues for the same value of J. The data in Figure 5 were fit using the empirical expression of Yang et al.[5] In eq 3, the variables were determined to be $A = -0.0213(5)$ MHz/Pa, $B = 0.036$ (8) MHz/Pa, $c_1 = -0.00022(3)$, $c_2 = 0.00020(4)$, and $c_3 = -3.7(3) \times 10^{-8}$.

$$\gamma = A + \frac{B}{1 + c_1 J' + c_2 J'^2 + c_3 J'^4} \qquad (3)$$

The self-broadening widths for the isotopologues are 4 (±2)% larger than the corresponding values that we found using FS-CRDS for $^{16}O_2$ (as reported in Robichaud et al.).[13] Previously, Gagliardi et al.[10] used FM spectroscopy to study the pressure-broadened line width with a Voigt profile for the R11 R11 transition of $^{18}O_2$ in a similarly ^{18}O-enriched sample. They monitored the line widths while varying the total pressure of the isotopically enriched sample and by adding various amounts of pure $^{16}O_2$ to a fixed quantity of the enriched sample. They observed the broadening parameter in the enriched bath gas to be 21 (±5)% larger than that in pure $^{16}O_2$. The corresponding $^{16}O_2$ self-broadening coefficient from HITRAN 2004[6] was in

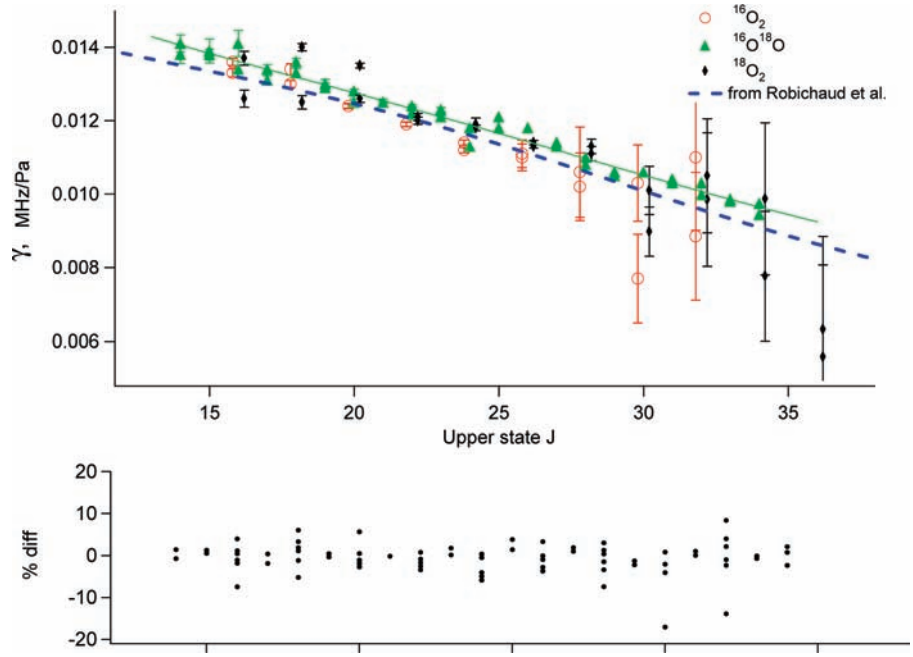

Figure 5. Self-broadening parameters as a function of upper state J for the isotopologues of the O_2 A-band in units of MHz/Pa at 296 K (note: 3.3798 cm^{-1} atm^{-1} = 1 MHz/Pa). Values for the different isotopologues are offset on the x-axis for clarity. The dashed blue line represents the self-broadening parameters from Robichaud et al.[13] The solid thin line represents fit to all the data shown based on eq 3 with coefficients of $A = -0.0213$ MHz/Pa, $B = 0.03646$ MHz/Pa, $c_1 = -0.0002153$, $c_2 = 0.0002016$, $c_3 = -3.675 \times 10^{-8}$. Present widths are approximately 4 (±2)% larger than corresponding values from Robichaud et al.[13] For the current data set, there is no discernible difference between the different isotopologues.

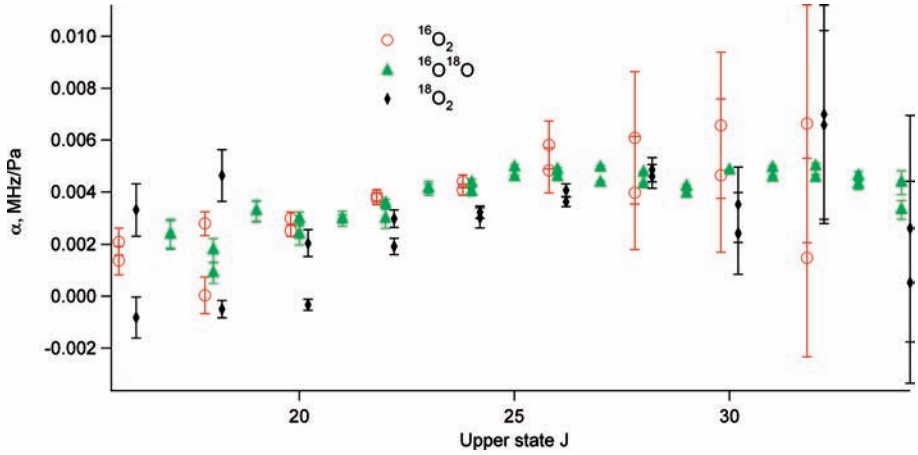

Figure 6. Collisional narrowing parameters as a function of upper state J for the isotopologues of the O_2 A-band in units of MHz/Pa. Values for the different isotopologues are offset on the x-axis for clarity. The values for the $^{16}O^{17}O$ and $^{17}O^{18}O$ isotopologues are not shown due to their large uncertainties. The narrowing parameters from the current study are 8 (±16) % smaller than the $^{16}O_2$ results in Robichaud et al.[13] There appears to be a slight lowering of the narrowing parameter with increasing mass of −0.0003 (1) (MHz/Pa)/amu.

the middle of the two determinations. Schermaul[12] used a nonstandard "collisionally narrowed Voigt" profile to fit their data and reported the $^{16}O_2$ self-broadening coefficients to be 24 (±10)% larger than the $^{16}O^{18}O$ broadening coefficients for broadening by $^{16}O_2$. Both studies invoked resonant exchange processes in the collisional model as the cause of the differential broadening between isotopologues, although Schermaul also suggested that the additional rotational states in $^{16}O^{18}O$ due to symmetry may play a role.

In contrast to the results of Gagliardi et al. and Schermaul, we find minimal differences in the line broadening of the isotopologues, though our experiments were done in enriched samples. In order to compare our results directly to those of Schermaul, we measured the broadening coefficients of three $^{16}O^{18}O$ lines (P19 P19, P17 P17, and P15 P15) in an O_2 sample with an isotopic composition near natural abundance. The measured $^{16}O^{18}O$ broadening coefficients were identical to the $^{16}O_2$ self-broadened coefficients for transitions having the same J to within their combined uncertainties and were (4 ± 1)% smaller than the corresponding coefficients for broadening by the ^{18}O-enriched gas mixture. A 20% change in broadening should have been detectable in our experiment, given our ability to see subtle line shape effects (e.g., collisional narrowing, speed dependence),[19] our precision, and the good agreement of our $^{16}O_2$ self-broadening coefficients with other high-resolution studies.[29] One probable explanation for the discrepancy between our work and that of Gagliardi et al.[10] and Schermaul[12] is line shape effects, particularly collisional narrowing.

Collisional narrowing parameters are shown in Figure 6 for the $^{16}O_2$, $^{16}O^{18}O$, and $^{18}O_2$ isotopologues. The $^{16}O^{17}O$ and $^{17}O^{18}O$

are not shown due to their larger uncertainties. Of the three isotopologues shown in Figure 6, there is a slight change in narrowing parameters for a given J of $-(0.0003 \pm 0.0001)$ (MHz/Pa)/amu when considering the highest precision data from $20 < J < 26$. This is in agreement with the collisional narrowing study of Ritter[28] in which he investigated the narrowing parameter for the series of noble gases. Ritter's work indicates a value of -0.0001 (MHz/Pa)/amu for the narrowing parameter, which is the same sign and order of magnitude as our study. Therefore, if the collisional narrowing parameter were considered constant for all of the isotopologues, the pressure broadening parameter would err on the order of a few percent depending on the isotopologues considered. This effect could account for the discrepancies in the pressure broadening parameter described above.

Conclusions

Experimental line parameters of the oxygen A-band are determined for the $^{16}O_2$, $^{16}O^{17}O$, $^{16}O^{18}O$, $^{17}O^{18}O$, and $^{18}O_2$ isotopologues. The $^{17}O_2$ isotopologue is not studied due to its low abundance and signal-to-noise. Molecular constants for the excited $b^1\Sigma g +$ states are obtained and are in good agreement with previous studies. In the 2004 edition of HITRAN,[6] the $^{16}O^{17}O$ line positions using the results of Camy-Peyret et al.[8] are in good agreement with our own findings, but the $^{16}O^{18}O$ line positions (based on the original work of Babcock and Herzberg[7]) are in significant disagreement with present and other results[9,11,12] by up to 0.3 cm^{-1} for $J' = 34$.

We find that self-broadening widths obtained from enriched ^{18}O samples are similar for the five isotopologues studied, and they are ~4% larger than the $^{16}O_2$-broadened coefficients of $^{16}O_2$ and $^{16}O^{18}O$. These results are in disagreement with Gagliardi et al.[10] and Schermaul[12] in that large differences in broadening coefficient are reported for the same isotopologue with a different bath gas and for different isotopologues broadened by the same bath gas. The use of simplistic line shape models (Voigt) or nonstandard profiles (collisionally narrowed Voigt) can account for these discrepancies. However, uncertainties in the experimentally determined collisional narrowing parameters preclude definite confirmation of this hypothesis. The results of the current work indicate that errors incurred by using the $^{16}O_2$ broadening parameters for the other isotopologues for the same J are negligible.

The $^{16}O_2$, $^{16}O^{18}O$, and $^{16}O^{17}O$ line parameters for the oxygen A-band have been extensively revised in the HITRAN 2008 database[30] using results from the present study and our earlier papers.[13−15] The current format of the database precludes the inclusion of narrowing coefficients, and we recommend that the measured values from the present paper be applied if needed. For applications that involve high optical densities and higher pressures, line mixing and collision-induced absorption should also be considered.[31]

Acknowledgment. Part of the research described in this paper was performed at the Jet Propulsion Laboratory, California Institute of Technology, under contract with The National Aeronautics and Space Administration (NASA). Additional support was provided by the Orbiting Carbon Observatory (OCO) project, a NASA Earth System Science Pathfinder (ESSP) mission; the NASA Upper Atmospheric Research Program grant NNG06GD88G; and the NIST Office of Microelectronics Programs. Laurence Y. Yeung would like to acknowledge the support of the Davidow Graduate Fellowship in Environmental Science. David A. Long acknowledges the support of the National Defense Science and Engineering Graduate Fellowship. Daniel K. Havey received support from the National Research Council as a postdoctoral fellow at NIST. Finally, we would like to acknowledge the assistance of Dr. Mona Shahgholi in performing the mass spectral analyses of our enriched gas sample.

References and Notes

(1) O'Brien, D. M.; English, S. A.; DaCosta, G. *J. Atmos. Oceanic Technol.* **1997**, *14*, 105.
(2) Chance, K. *J. Quant. Spectrosc. Radiat. Transfer* **1997**, *58*, 375.
(3) Corradini, S.; Cervino, M. *J. Quant. Spectrosc. Radiat. Transfer* **2006**, *97*, 354.
(4) van Diedenhoven, B.; Hasekamp, O. P.; Aben, I. *Atmos. Chem. Phys.* **2005**, *5*, 2109.
(5) Yang, Z.; Wennberg, P. O.; Cageao, R. P.; Pongetti, T. J.; Toon, G. C.; Sander, S. P. *J. Quant. Spectrosc. Radiat. Transfer* **2005**, *90*, 309.
(6) Rothman, L. S.; Jacquemart, D.; Barbe, A.; Benner, D. C.; Birk, M.; Brown, L. R.; Carleer, M. R.; Chackerian, C.; Chance, K.; Coudert, L. H.; Dana, V.; Devi, V. M.; Flaud, J. M.; Gamache, R. R.; Goldman, A.; Hartmann, J. M.; Jucks, K. W.; Maki, A. G.; Mandin, J. Y.; Massie, S. T.; Orphal, J.; Perrin, A.; Rinsland, C. P.; Smith, M. A. H.; Tennyson, J.; Tolchenov, R. N.; Toth, R. A.; Vander Auwera, J.; Varanasi, P.; Wagner, G. *J. Quant. Spectrosc. Radiat. Transfer* **2005**, *96*, 139.
(7) Babcock, H. D.; Herzberg, L. *Astrophys. J.* **1948**, *108*, 167.
(8) Camy-Peyret, C.; Payan, S.; Jeseck, P.; Te, Y.; Hawat, T. *Proceedings of the International Radiation Symposium, Saint Petersburg, Russia*, 2000; Paper E4.
(9) van Leeuwen, N. J.; Kjaergaard, H. G.; Howard, D. L.; Wilson, A. C. *J. Mol. Spectrosc.* **2004**, *228*, 83.
(10) Gagliardi, G.; Gianfrani, L.; Tino, G. M. *Phys. Rev. A* **1997**, *55*, 4597.
(11) Naus, H.; de Lange, A.; Ubachs, W. *Phys. Rev. A* **1997**, *56*, 4755.
(12) Schermaul, R. *J. Quant. Spectrosc. Radiat. Transfer* **1999**, *62*, 181.
(13) Robichaud, D. J.; Hodges, J. T.; Brown, L. R.; Lisak, D.; Maslowski, P.; Okumura, M.; Miller, C. E. *J. Mol. Spectrosc.* **2008**, *248*, 1.
(14) Robichaud, D. J.; Hodges, J. T.; Lisak, D.; Miller, C. E.; Okumura, M. *J. Quant. Spectrosc. Radiat. Transfer* **2008**, *109*, 435.
(15) Robichaud, D. J.; Hodges, J. T.; Maslowski, P.; Yeung, L. Y.; Okumura, M.; Miller, C. E.; Brown, L. R. *J. Mol. Spectrosc.* **2008**, *251*, 27.
(16) Hodges, J. T.; Ciurylo, R. *Rev. Sci. Instrum.* **2005**, *76*, 023112.
(17) Hodges, J. T.; Layer, H. P.; Miller, W. W.; Scace, G. E. *Rev. Sci. Instrum.* **2004**, *75*, 849.
(18) Hodges, J. T.; Lisak, D. *Appl. Phys. B: Laser Opt.* **2006**, *85*, 375.
(19) Lisak, D.; Hodges, J. T.; Ciurylo, R. *Phys. Rev. A* **2006**, *73*, 012507.
(20) Lisak, D.; Hodges, J. T. *Appl. Phys. B: Laser Opt.* **2007**, *88*, 317.
(21) Halmer, D.; von Basum, G.; Hering, P.; Murtz, M. *Rev. Sci. Instrum.* **2004**, *75*, 2187.
(22) Galatry, L. *Phys. Rev.* **1961**, *122*, 1218.
(23) Rouillé, G.; Millot, G.; Saint-Loup, R.; Berger, H. *J. Mol. Spectrosc.* **1992**, *154*, 372.
(24) Cazolli, G.; Degli Esposti, C.; Favero, P. G.; Severi, G. *Nuovo Cimento B* **1981**, *62*, 243.
(25) Mizushima, M.; Yamamoto, S. *J. Mol. Spectrosc.* **1991**, *148*, 447.
(26) Steinbach, W.; Gordy, W. *Phys. Rev. A* **1975**, *11*, 729.
(27) Gamache, R. R.; Goldman, A.; Rothman, L. S. *J. Quant. Spectrosc. Radiat. Transfer* **1998**, *59*, 495.
(28) Ritter, K. J. *A High-Resolution Spectroscopic Study of Absorption Line Profiles in the A-band of Molecular Oxygen*; University of Maryland, 1986.
(29) Brown, L. R.; Plymate, C. *J. Mol. Spectrosc.* **2000**, *199*, 166.
(30) Rothman, L. S.; Gorden, I. E.; Barbe, A.; Benner, D. C.; Bernath, P. F.; Birk, M.; Boudon, V.; Brown, L. R.; Campargue, A.; Champion, J.-P.; Chance, K.; Coudert, L. H.; Dana, V.; Devi, V. M.; Fally, S.; Flaud, J.-M.; Gamache, R. R.; Goldman, A.; Jacquemart, D.; Kleiner, I.; Lacome, N.; Lafferty, W. J.; Mandin, J.-Y.; Massie, S. t.; Mikhailenko, S.; Miller, C. E.; Moazzen-Ahmadi, N.; Naumenko, O. V.; Nikitin, A.; Orphal, J.; Predoi-Cross, A.; Perevalov, V.; Perrin, A.; Rinsland, C. P.; Rotger, M.; Šimečková, M.; Smith, M. A. H.; Sung, K.; Tashkun, S.; Tennyson, J.; Toth, R. A.; Vandaele, A. C.; Vander Auwera, J. *J. Quant. Spectrosc. Radiat. Transfer* **2009**, *110*, 533.
(31) Tran, H.; Hartmann, J.-M. *J. Geophys. Res.* **2008**, *113*, D18104.

JP901127H